

Numerical Modeling of Orthogonal Cutting: Application to Woodworking with a Bench Plane

John A. Nairn

John.Nairn@oregonstate.edu

Wood Science & Engineering, Oregon State University, Corvallis, OR 97331, USA

Submitted to Interface Focus: 29 Dec 2015, revised and accepted: 9 Feb 2016

Abstract

A numerical model for orthogonal cutting using the material point method (MPM) was applied to woodcutting using a bench plane. The cutting process was modeled by accounting for surface energy associated with wood fracture toughness for crack growth parallel to the grain. By using damping to deal with dynamic crack propagation and modeling all contact between wood and the plane, simulations could initiate chip formation and proceed into steady-state chip propagation including chip curling. Once steady state conditions were achieved, the cutting forces became constant and could be determined as a function of various simulation variables. The modeling details included a cutting tool, the tool's rake and grinding angles, a chip breaker, a base plate, and a mouth opening between the base plate and the tool. The wood was modeled as an anisotropic elastic-plastic material. The simulations were verified by comparison to an analytical model and then used to conduct virtual experiments on wood planing. The virtual experiments showed interactions between depth of cut, chip breaker location, and mouth opening. Additional simulations investigated the role of tool grinding angle, tool sharpness, and friction.

Keywords: Cutting, Wood, Material Point Method, Numerical Modeling, Cohesive Zone Modeling

Introduction

Cutting of materials always involves separation of two surfaces and inclusion of surface energy for that separation (*i.e.*, the material's fracture toughness) into models has led to new insights about cutting [1-4]. For example, Atkins [1] shows that incorporating surface fracture energy into models can explain several longstanding issues, such as material dependence of the shear plane angle, that have eluded historical methods based on plasticity and friction alone. Incorporating fracture energy also predicts that cutting force as a function of depth of cut should have a non-zero intercept [1,4]. This prediction is consistent with many cutting experiments. Furthermore, if the non-zero intercept is found by extrapolating cutting force per unit width of cut, the intercept is equal to the material's fracture toughness [1,4]. Several groups have exploited this observation to measure fracture toughness of materials using instrumented cutting experiments [5-8]. This approach is particularly attractive for materials where it is difficult to achieve crack propagation with remote loading, such as soft materials [7,9]. The cutting tool enters the material and provides crack propagation. Analyzing the resulting cutting forces as a function depth of cut can provide information about toughness and potentially other material properties [6,9].

Including fracture surface energy in analytical or numerical models opens up new potential for those models to improve realism. For example, Williams et al. [9,10] developed analytical models for orthogonal cutting with crack propagation including plastic shearing and plastic bending modes. The initial model was for isotropic materials with elastic plastic behavior, although it is easily extended to plastic hardening [11]. The addition of explicit crack growth is also an important concept for numerical modeling. Many past numerical models have focused on plasticity behavior, but because cutting cannot progress without separating elements (in finite element methods), most had to introduce *ad hoc* separation criteria [1]. When explicit crack growth is directly included in the model, those separation criteria can be based on physically justifiable fracture mechanics criteria [1]. For example, Ref. [11] describes a material point method (MPM) simulation of orthogonal cutting. The crack growth was modeling by explicit crack growth using cohesive zone methods. This numerical scheme was able to simulate full chip formation and propagation into steady state cutting conditions for both plastic shearing and plastic bending modes. The contact capabilities of MPM were helpful for providing stable simulations even when the tool tip touches the crack tip (*e.g.*, when the gap between the tool tip and crack tip shown in Fig. 2 below disappears).

One motivation for developing numerical simulations of cutting is to handle complexities that are beyond the capabilities of analytical models. For example, Fig. 1 shows a woodworking bench plane (or Jack plane) and Fig. 2 shows geometry of the cutting region of such a plane including a cutting tool, a chip breaker, and a base plate (or sole). This problem introduces several complexities. First, the material being cut (wood) is an anisotropic material with anisotropic plasticity and failure criteria. Second, a chip breaker and base plate introduce new contact surfaces that will influence the cutting process. Third, with the additional contact surfaces, frictional contact may become more important and may need to involve non-Coulomb friction processes. All these issue, and more, can potentially be included into numerical simulations of cutting.

This work's goal was to demonstrate that MPM modeling can incorporate sufficient realism into cutting models to develop computer simulations for analyzing a wood working bench plane. Such simulations can then be used to optimize wood planing, which has historically been done through trial and error. Some examples are the importance of tool angles, the proper adjustments that should be made to set chip breaker location or mouth opening, the effect of planing direction in the wood (with the grain or cross grain), the role of friction on all surfaces, and the effects of tool sharpness. This paper describes an MPM model for a bench plane and addresses several of these issues. The new features in this paper compared to Ref. [11] are to model cutting of an anisotropic material (wood) and to incorporate realistic effects of cutting equipment, such as a chip breaker and a base plate in a bench plane.



Figure 1. A picture of a typical bench plane or Jack plane. (from <http://4mechtech.blogspot.com/2013/12/Jack-plane.html>).

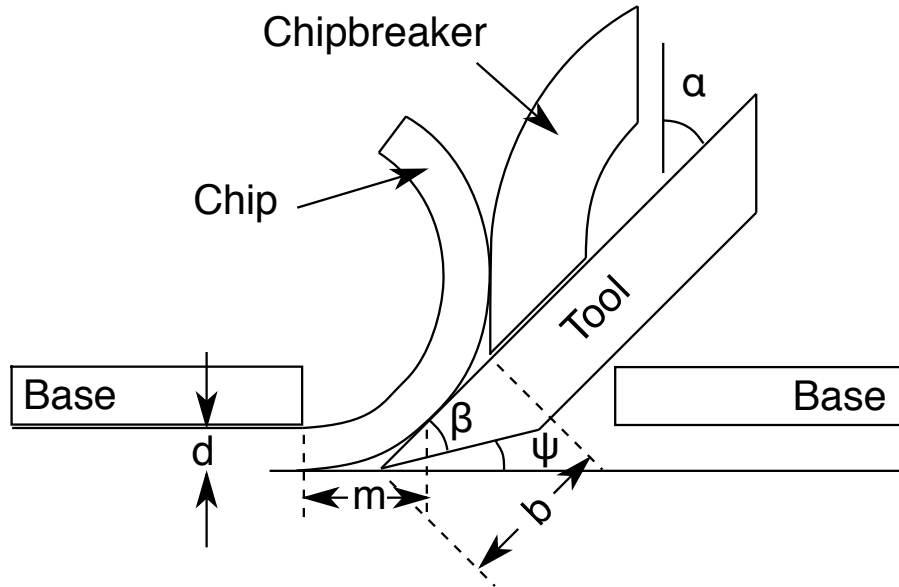


Figure 2. Key geometric features of a bench plane showing a cutting tool, a base plate of the plane, and the beginning of a chip breaker; α , β , and ψ are rake, grinding, and clearance angles, respectively; d , m , and b are depth of cut, mouth opening, and chip breaker location, respectively.

Materials and methods

Numerical Modeling

This numerical model for wood planing used the material point method (MPM). The details for MPM modeling of orthogonal cutting are given in Ref. [11]. This section summarizes some key points and describes additions needed for modeling a bench plane. MPM is a particle-based method for computational mechanics [12,13]. It is analogous to finite element method (FEM), but the particle nature gives it different properties for certain problems. In particular, MPM has some advantages for modeling problems involving large deformations [14], explicit cracks [15-17], and contact [18-20]. All these issues are present when modeling cutting using explicit fracture criteria for crack growth.

The wood material was modeled as an orthotropic, elastic-plastic material in 2D plane-strain conditions. The orthotropic symmetry directions in wood are the longitudinal or grain direction (L), radial direction (R), and tangential directions (T). These directions refer to cylindrical tree structure, but when modeling a board, wood is usually treated as approximately rectilinearly orthotropic depending on how it was cut from the tree. Figure 3 shows approximately “RL” and “TL” boards to be planed in the grain direction along the top narrow edge indicated with dashed lines. The first letter is the normal to the narrow edge (and the cut plane) while the second letter is the cutting direction. The simulations here assigned properties similar to Douglas-fir softwood [21-23] and are given in Table 1. For RL, the directions are $x = L$, $y = R$, and $z = T$ and for TL they are $x = L$, $y = T$, and $z = R$. RL boards correspond to radial sawn boards while TL boards are flat sawn. Approximately TL boards are more common and are emphasized in these simulations.

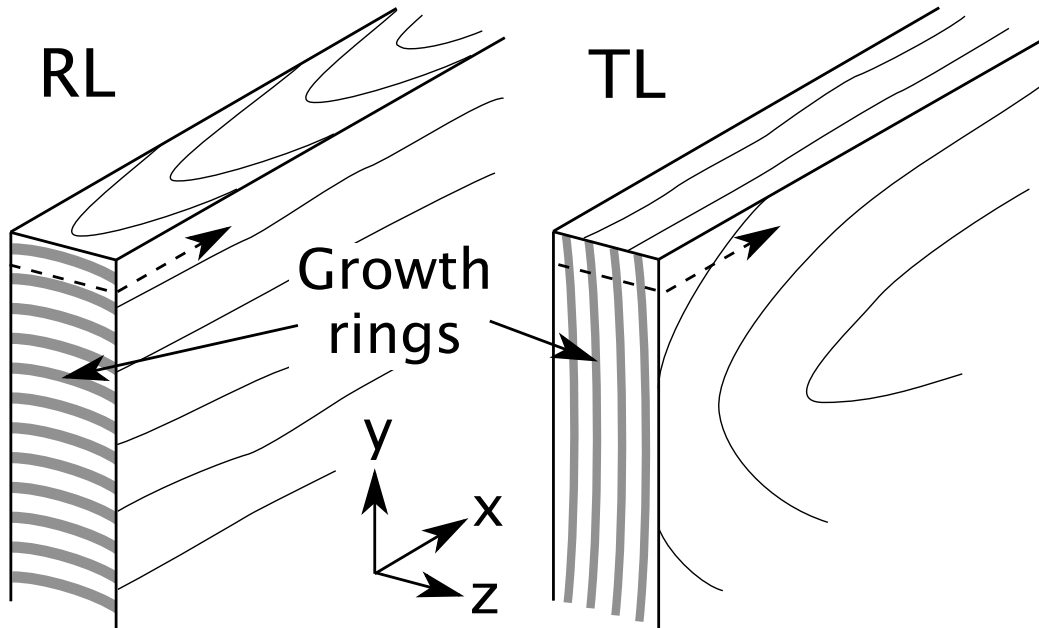


Figure 3. The growth ring orientations for two board types to be planed along the top narrow edge. RL and TL indicate top surface normals in the radial direction (R) and tangential direction (T) with planing to be in the longitudinal direction (L). The x - y - z coordinate axes show the coordinates used in the numerical simulations.

Table 1. Elastic, plastic, and fracture properties of Douglas-fir wood for simulations of planing in the TL and RL directions.

Property	TL	RL
E_L , E_R , and E_T (MPa)	14500, 960, and 620	
G_{LR} , G_{LT} , and G_{TR} (MPa)	830, 760, and 80	
ν_{LR} , ν_{LT} , and ν_{LR}	0.37, 0.42, and 0.35	
$\sigma_{Y,LL}$, $\sigma_{Y,RR}$, and $\sigma_{Y,TT}$ (MPa)	100, 10, and 10	
$\tau_{Y,LR}$, $\tau_{Y,LR}$, and $\tau_{Y,TR}$ (MPa)	30, 30, and 4	
K and n	2 and 1	
Mode I G_{init} and G_b (J/m ²)	215 and 405	158 and 0
Mode I σ_c and σ_b (MPa)	4.65 and 0.8	6.24 and 0
Mode I δ_1/δ_c and δ_2/δ_c	0.05 and 0.1	0.1 and 1
Mode I δ_c (mm)	1.0125	0.051
Mode II G_{total} (J/m ²)	645	474
Mode II σ_c (MPa)	4.65	6.24
Mode II δ_c (mm)	0.278	0.152

To account for anisotropic plastic properties of wood, especially the large difference between yielding parallel and perpendicular to the grain, the wood was modeled as a Hill plastic material [24] with yielding criterion:

$$\sqrt{F(\sigma_{xx} - \sigma_{yy})^2 + G(\sigma_{xx} - \sigma_{zz})^2 + H(\sigma_{yy} - \sigma_{xx})^2 + \frac{\tau_{yz}^2}{\tau_{Y,yz}^2} + \frac{\tau_{xx}^2}{\tau_{Y,xz}^2} + \frac{\tau_{xy}^2}{\tau_{Y,xy}^2}} = 1 + K\varepsilon_p^n$$

where

$$F = \frac{1}{2} \left(\frac{1}{\sigma_{Y,yy}^2} + \frac{1}{\sigma_{Y,zz}^2} - \frac{1}{\sigma_{Y,xx}^2} \right) \quad G = \frac{1}{2} \left(\frac{1}{\sigma_{Y,xx}^2} + \frac{1}{\sigma_{Y,zz}^2} - \frac{1}{\sigma_{Y,yy}^2} \right)$$

$$H = \frac{1}{2} \left(\frac{1}{\sigma_{Y,xx}^2} + \frac{1}{\sigma_{Y,yy}^2} - \frac{1}{\sigma_{Y,zz}^2} \right)$$

Here σ_{ii} and τ_{ij} are current stresses, $\sigma_{Y,ii}$ and $\tau_{Y,ij}$ are material yield strengths for loading in one direction, ε_p is cumulative plastic strain, and K and n are material hardening parameters. The yield strengths for Douglas-fir wood, which are based on failure loads in the different directions [21,22], are given in Table 1. This small-strain material used approximate polar decomposition methods to allow for large displacements and rotations during chip formation (*i.e.*, a standard hypoelastic material implementation [25]).

The cutting region geometry for a bench plane with a “bevel-down” style blade is shown in Fig. 2. The most important features are the cutting tool, a chip breaker, and a base plate (or sole). The rake angle, α , is typically fixed at 45°. The tool bevel or grinding angle, β , is set when sharpening the tool and common wood recommendations are to grind the bevel between 25° and 30°. The remaining clearance angle is $\psi = 90 - \alpha - \beta$. Different plane conditions can be modeled by adjusting tool angles, by adjusting distance to the chip breaker (b), or by setting the mouth opening (m).

A challenge in modeling cutting is dealing with all the contact situations. Although MPM handles contact well, its accuracy is determined by accuracy in determining the normals on contacting surfaces [19,20]. When possible, the contact normal on the tool was set using the input rake angle while the contact normal on the base plate and bearing surfaces was set to vertical. But, as the geometry of the plane gets more complex, more surfaces may come into contact making it difficult to hard code simple contact angles. Thus, when the simulations added a chip breaker and a base plate or when the tool was modeled with rounded edge to model a blunt tool, all contact normals were calculated by MPM methods based on volume gradients of the materials [19,20]. Because the tool was modeled as a rigid material (see below), its surface normals should be more reliable than normals calculated from the highly deforming cut material. Thus, the contact normals were calculated from the volume gradients of the tool material whenever possible [19]. The contact was either frictionless or added Coulomb friction.

A challenge combining contact and cracks in MPM is to allow the tool material to be inside the crack but to only allow the MPM explicit crack algorithm [15] to affect the material being cut. This challenge is most easily met with rigid materials [11]. Therefore, all components of the plane were modeled as rigid materials (note: modeling effects such as tool wear would require use of non-rigid materials in cracks, which will be the subject of future work). As explained in

Ref. [11], the rigid material velocity was ramped up to 2 m/sec and a kinetic energy “thermostat” [26] was used to control start-up inertial effects. After reaching final velocity, the damping thermostat was turned off and the cutting soon established steady state conditions. All cutting forces were evaluated from simulation forces during this steady state phase. Note that 2 m/sec is much faster than ever expected with a hand bench plane, but this speed is much slower than the longitudinal wave speed in the wood (about 6000 m/sec) and therefore sufficiently slow to model quasi-static cutting. Because the orthotropic, elastic-plastic material model has no inherent rate dependence, the numerical results would not change at slower speeds. A numerical model to study such rate effects in cutting would require new material models that capture the underlying rate dependence of wood.

Explicit crack propagation was modeled using MPM cohesive zones [11,27,28]. In brief, an initial crack was introduced along the entire cutting path and the crack plane was modeled with a cohesive law determined by fracture experiments in the appropriate failure plane for solid wood (see below). This approach limited simulations to straight crack growth and therefore could not model chip fracture caused by fracture paths diverting toward the surface [4].

All numerical models simulating dynamic crack growth must incorporate a scheme for extending the crack. For example, in FEM, a node is released in the crack plane or in explicit MPM cracks the crack path is extended by a small amount [15,16]. Even in cohesive zone modeling, a crack grows when the crack opening displacement at the crack root reaches the cohesive law’s critical value (δ_c) and traction drops to zero. In computational mechanics code that correctly conserves total energy, all these virtual crack extension can cause an increase in kinetic energy that can quickly deteriorate numerical results. But, this conversion to kinetic energy does not reflect crack extension in real materials where that energy is instead absorbed by some surface processes representing the material’s fracture toughness. One solution to dealing with artifacts in dynamic crack propagation simulations is to add damping to mimic energy absorption in real materials, but it is challenging to add realistic damping. In previous orthogonal cutting simulations, it was noticed that a new form of damping, denoted as PIC damping [11], worked very well for crack propagation simulations. In brief, this damping focuses damping effects in regions with high velocity gradients and therefore selectively dampens regions around a propagating crack tip. Simulations with PIC damping enabled are extremely stable for all cutting conditions, while simulations without PIC damping were only stable for a few conditions. When they both work, they give nearly identical cutting forces except for far less noise when using PIC damping. All simulations here used the PIC damping method [11].

Finally, resolution (which used 15 particles in the thickness direction of the chips) and boundary conditions (fixed displacements on the bottom) were selected using the same methods as in Ref [11]. Each simulation propagated the cut surface a distance equal to 50 times the depth of cut. Typical simulations took 30 hours using 20 cores on computer nodes with Intel® Xeon® E5-2698 v3 processors and the MPM software OSParticulas [29]. More than one third the processing time was numerically solving equations to implement anisotropic plasticity. Work in progress may improve efficiency for this task.

Analytical Modeling

Due to the high longitudinal stiffness of wood when planing in the grain direction, woodcutting is predominantly in the plastic bending mode where the tool wedges open the crack but the tool tip does not reach the crack tip (see crack tip region in Fig. 2). Williams *et al.* [9,10] derived an analytical model for cutting by plastic bending. Nairn [11] extended that model to

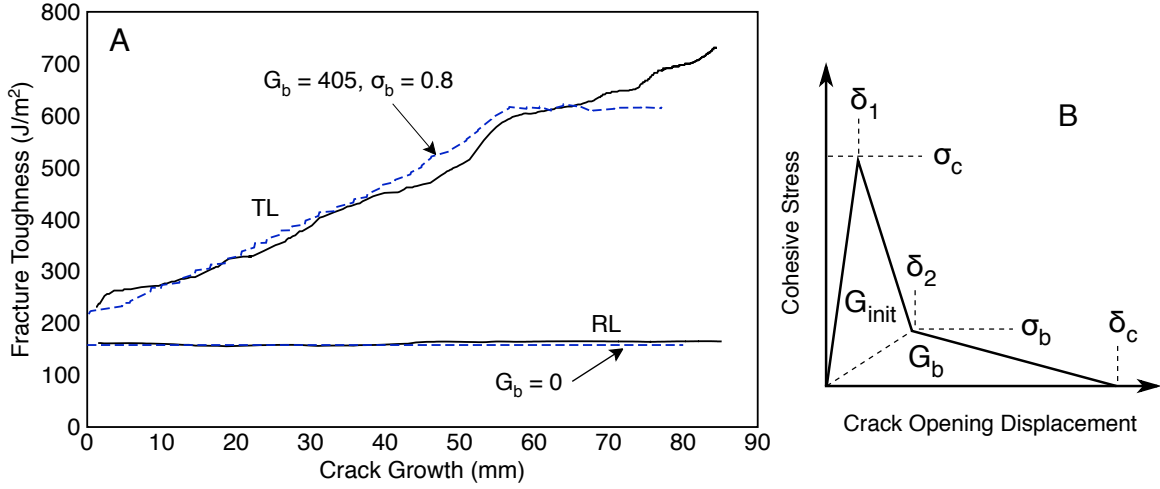


Figure 4. A. Experimental results for Douglas-fir mode I fracture in the TL and RL directions. The dashed lines are numerical simulations assuming fracture initiation followed by linear softening fiber bridging. B. Trilinear traction law used to model crack propagation in cutting simulations.

allow for plastic hardening and to account for bearing forces seen on the bottom of the tool in numerical solutions. The plastic bending analysis includes a χ factor introduced by Williams [30] to account for crack-root rotation effects. For isotropic materials $\chi = 0.67$, but it changes to

$$\chi = \sqrt{\frac{E_{xx}}{11G_{xy}} \left[3 - 2 \left(\frac{\Gamma}{1 + \Gamma} \right)^2 \right]} \quad \text{and} \quad \Gamma = 1.18 \frac{\sqrt{E_{xx}E_{yy}}}{G_{xy}}$$

for anisotropic materials where x and y refer to cutting and transverse directions, respectively. For planing wood in the grain direction (and using plane-strain properties deduced from Table 1 properties), $\chi_{RL} = 1.59$ and $\chi_{TL} = 1.7$. Analytical calculations done here for RL cutting used this χ_{RL} , estimated bearing forces from numerical results, and used the expressions given in section 3 of Ref. [11] to find cutting forces

Results and discussion

Solid Wood Fracture Properties

One goal of numerical simulations for cutting wood is to predict how cutting and machining methods change with wood properties. Then, by using wood fracture properties for different wood species or for wood under various conditions (*e.g.*, temperature and moisture content), one could optimize machining techniques. To model wood planing, the first need was to know Douglas-fir fracture properties for crack growth in the RL and TL modes. Matsumoto and Nairn [31] did those experiments using compact tension specimens; their experimental results are shown in Fig. 4A (solid lines). For both RL and TL directions, the fracture initiates at a low value (150-200 J/m²) and then increases as a function of crack length (which is known as the material's R curve). The increases in toughness are likely caused by fiber bridging. The increase for RL crack growth was small, but was dramatic for TL growth. A physical interpretation is that TL fiber bridging is much more effective at increasing toughness because it includes fibers from

the higher-density late wood zones in the growth rings (*i.e.*, the crack front spans the growth rings — see Fig. 3). In contrast, an RL crack can remain mostly within a single low-density, early wood region and those fibers are less effective at increasing toughness.

To implement these fracture properties into modeling based on cohesive zones, the experimental results were fit to a fracture model that assumes fracture initiations at some initiation toughness (G_{init}) and then toughness increases due to fiber bridging in the wake of the crack tip and modeled by a linear softening behavior with total bridging toughness G_b [27,31]. The TL experiments could be fit to an MPM crack propagation simulation [31] using $G_{init} = 215 \text{ J/m}^2$ and $G_b = 405 \text{ J/m}^2$. The RL experiments could be fit well enough with $G_{init} = 158 \text{ J/m}^2$ and no bridging (fits are dashed lines in Fig. 4). Alternatively, Douglas-fir fracture behavior can be modeled solely with a cohesive law by using the trilinear cohesive law shown in Fig. 4B. Such a law can represent two physical mechanisms. The high first peak represents fracture initiation while the long tail is softening behavior due to fiber bridging. The triangular areas under these peaks are:

$$G_{init} = \frac{1}{2}(\sigma_c \delta_2 - \sigma_b \delta_1) \quad \text{and} \quad G_b = \frac{1}{2}\sigma_b \delta_c$$

The resulting cohesive law properties derived from these experiments and used for cutting simulations are given Table 1. Although experiments provide G_{init} and G_b , the specific values for cohesive stresses and critical crack opening displacements are less certain. Some consequences of changing these values are discussed below and in Ref. [11].

The experiments from Ref. [31] were mode I failure, but cutting is not pure mode I. Although mode II R curves are not available for Douglas-fir wood, experiments on Balsa wood suggest mode II initiation toughness is about three times higher than mode I and that mode II crack propagation is unaffected by fiber bridging [32]. These cutting simulations therefore set mode II toughness to three times the mode I initiation toughness and ignored fiber bridging effects (the mode II cohesive law properties are in Table 1).

Finally, for mixed-mode failure, the cohesive law was determined to have failed using a decoupled elliptical failure criterion [33]:

$$\left(\frac{G_I}{G_{Ic}}\right)^n + \left(\frac{G_{II}}{G_{IIc}}\right)^m = 1 \quad (1)$$

where G_I and G_{II} are areas under the cohesive law up to the current normal and tangential crack opening displacements, respectively, and G_{Ic} and G_{IIc} are total areas under the mode I and mode II cohesive laws. For simplicity, all simulations here used $n = m = 1$. When the crack grows, the mode I character of the crack growth is given by $G_I/(G_I+G_{II})$. Simulations show that wood planing is predominantly mode I, but ranged from 65% to 99% mode I depending on various cutting parameters.

Verification Simulations

In numerical modeling, it is important to verify simulation methods by comparison to known solutions, such as analytical models. Unfortunately, no model is available for cutting wood with anisotropic yielding, but if the failure is converted to an isotropic von Mises yield criterion (by setting $\sigma_{Y,xx} = \sigma_{Y,yy} = \sigma_{Y,zz} = \sigma_Y$ and $\tau_{Y,ij} = \sigma_Y/\sqrt{3}$), numerical results can be compared to the Williams *et al.* [9,10] analytical model provided χ is adjusted for anisotropic material properties

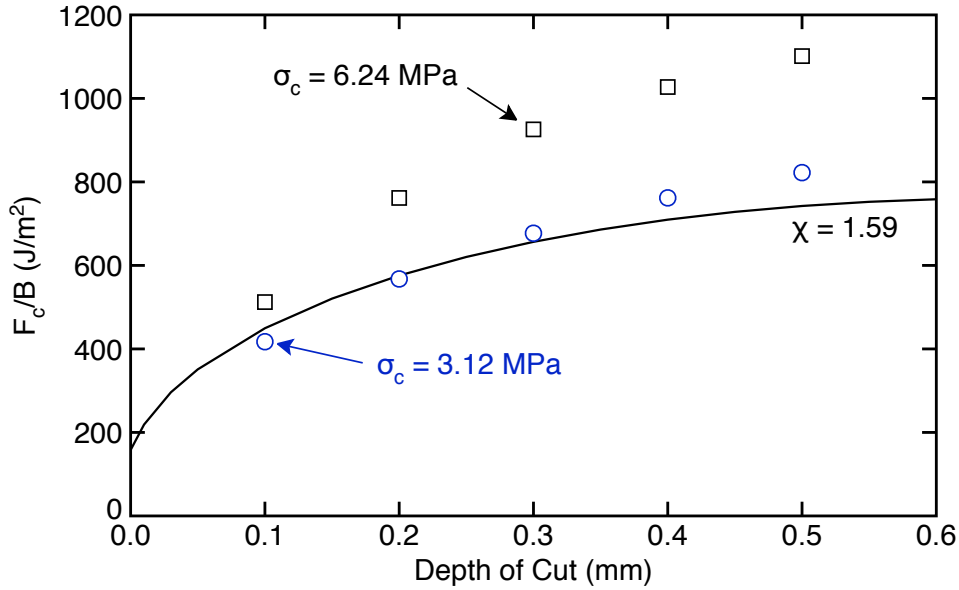


Figure 5. Cutting force, F_c , per unit width (B) as a function of depth of cut for RL cutting using an isotropic yield strength ($\sigma_Y = 60$ MPa). The symbols are numerical simulations for two different cohesive stresses but constant $G_{total} = 158$ J/m². The solid line is analytical model for an anisotropic material with isotropic yielding.

and the model is modified to account for bearing forces observed in simulation results [11]. The results for simulation of RL fracture as a function of depth of cut using $\sigma_Y = 60$ MPa are in Fig 5. To better match analytical modeling assumptions, the RL cohesive law for mode II was changed to match the RL mode I cohesive law in Table 1 such that the crack always propagates at constant $G_c = 158$ J/m² (see Eq. (1)). These initial results were 20 to 40% higher than the analytical model (solid line), but changing the cohesive stress could eliminate the entire difference. By reducing the cohesive stress by a factor of two (to $\sigma_c = 3.12$ MPa) while maintaining constant overall toughness (by doubling δ_c), the numerical and analytical models agreed well. Although these simulations verify the the sensitivity of results to details of cohesive law parameters raises concerns about reliance on cohesive zone models without sufficient validation of all its parameters.

Bare Cutting Tool

These simulations switched to TL planing and restored anisotropic yielding properties. The TL mode is more common in lumber and also has more fiber bridging effects. In fact, the fiber bridging is so extensive that the tool enters the fiber-bridging zone (as shown in Fig. 6A). This situation raises another issue with cohesive zone modeling. If a tool enters a cohesive zone and that zone is meant to represent a real physical process, like fiber bridging, one might expect that the tool will alter the cohesive zone process. For fiber bridging in wood, one might expect that the tool will cut the bridging fibers. Figure 6B shows steady state chip formation for a simulation in which the cohesive zone fails if it either reaches critical crack opening displacement or if the leading edge of the tool crosses the current location of the zone/crack particle.

To assess the effects of cutting the cohesive zone, Fig. 7 compares cutting forces as function of depth of cut for simulations in which the tool either ignores or cuts the bridging fibers.

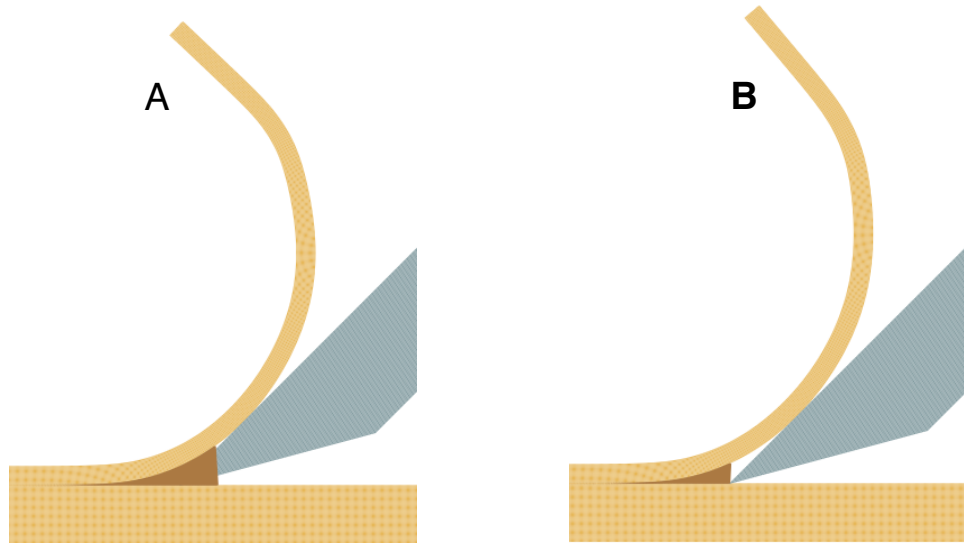


Figure 6. Steady state chips for TL planing. A. Simulation where the tool is allowed to enter the cohesive zone. B. Simulation where the tool's leading edge cuts the bridging fibers in the cohesive zone.

Because some of wood's toughness is due to fiber bridging [31], when the tool cuts that zone, the effective toughness is reduced, as are the total cutting forces. Extrapolating to zero depth of cut (using quadratic fits), a tool that ignores the zone extrapolates to the expected total mode I toughness (area under the cohesive law). When the tool cuts the zone, however, the force extrapolates to close to the mode I initiation toughness. In other words, the tool has eliminated most of the Douglas-fir toughness attributed to fiber bridging. The difference between the two curves was larger for thin cuts because the tool gets closer to the crack tip and therefore when the

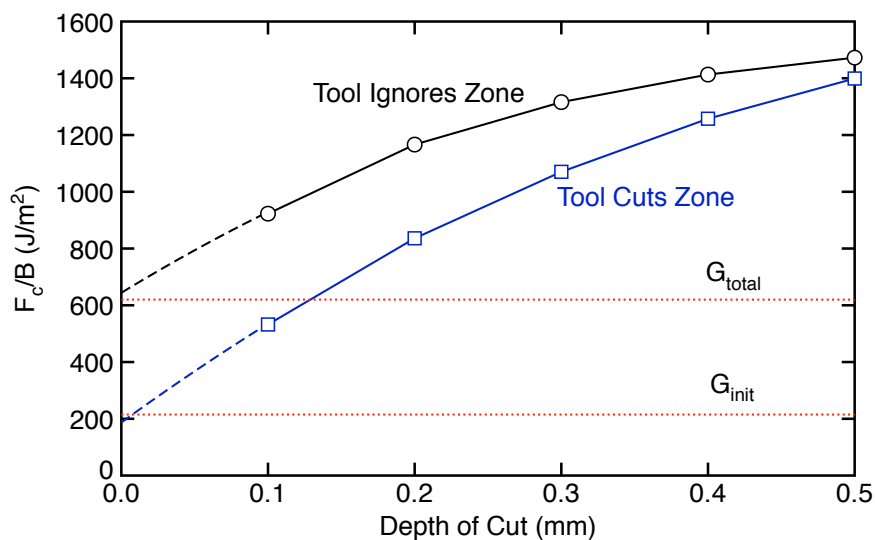


Figure 7. Cutting force, F_c , per unit width (B) as a function of depth of cut for TL planing for simulations where the tool either ignores or cuts the cohesive zone. The dashed extensions are quadratic extrapolations to zero depth of cut. The horizontal lines are for total mode I toughness and initiation mode I toughness.

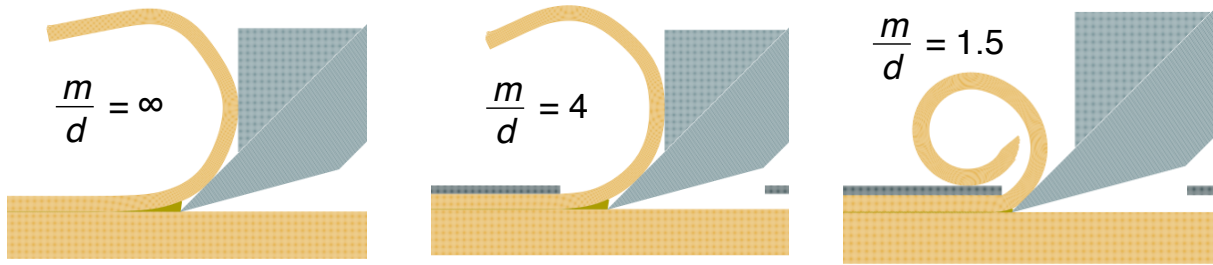


Figure 8. Steady state chips for TL planing when using a chip breaker located 1.59 mm from the tool tip for depth of cut of 0.3 mm and for various mouth openings.

tool cuts the zone, more bridging fibers are cut. These simulations highlight an important difference between remote-loading fracture experiments and fracture experiments based on cutting experiments. Although both are controlled by the material's toughness, if a cutting tool alters a process zone around the crack tip, such as cutting bridging fibers, the toughness measured by cutting may differ from (and likely be lower than) the toughness measured by remote loading.

Add Chip Breaker and Base Plate

Because of wood's high longitudinal stiffness in the grain direction, the steady state chips formed with the tool alone have low curvature and the crack tip has potential to be far ahead of the tool tip (see Fig. 6). Adding a chip breaker and base plate will alter the process. A chip breaker, if positioned correctly, will force the chip to curl. A base plate will put downward pressure on the wood preventing the crack from propagating too far from the tool perhaps enhancing control of the cutting process. The next simulations added a chip breaker and a base plate. The chip breaker was positioned $b = 1.59$ mm (1/16 inch) from the tool tip. Only a small and approximately vertical portion of the chip breaker was needed because only that region contacts the chip. The base plate was added to give various mouth openings (m). Only the base plate in front of the tool tip contacts the wood.

Figure 8 shows steady state chips for a 0.3 mm depth of cut, constant chip breaker position ($b = 1.59$ mm) and variable ratio of mouth opening to the depth of cut. With no base plate ($m/d = \infty$), the chip runs up the tool but then is bent by the chip breaker. The resulting chip curvature is much higher than without a chip breaker (*c.f.*, chips in Fig. 6). These simulations used anisotropic yielding with plasticity and therefore had no scheme to actually break the chip or to draw conclusions about ideal chip shape for smooth cuts, but the effect of the chip breaker is captured by its large affect on increased final chip curvature. The extra chip curvature when $m/d = \infty$ is only slightly modified when $m/d = 4$, but when $m/d = 1.5$ the chip curvature is greatly increased and no longer even contacts the chip breaker. It was not possible to run simulations with $m/d = 1$ or less because the chip did not fit through the opening. These simulations indicate that both chip breaker location and mouth opening affect chip curvature and they interact. When the mouth opening is narrow, the chip breaker serves no function unless it is moved sufficient close to the tool tip.

Figure 9 shows steady state chips as a function of the depth of cut (from 0.05 mm to 0.5 mm) for constant chip breaker location ($b = 1.59$ mm) and constant mouth opening ($m = 1.2$ mm, which means m/d varied from 24 to 2.4). For depths of cut 0.05 and 0.1 mm, the chips curl

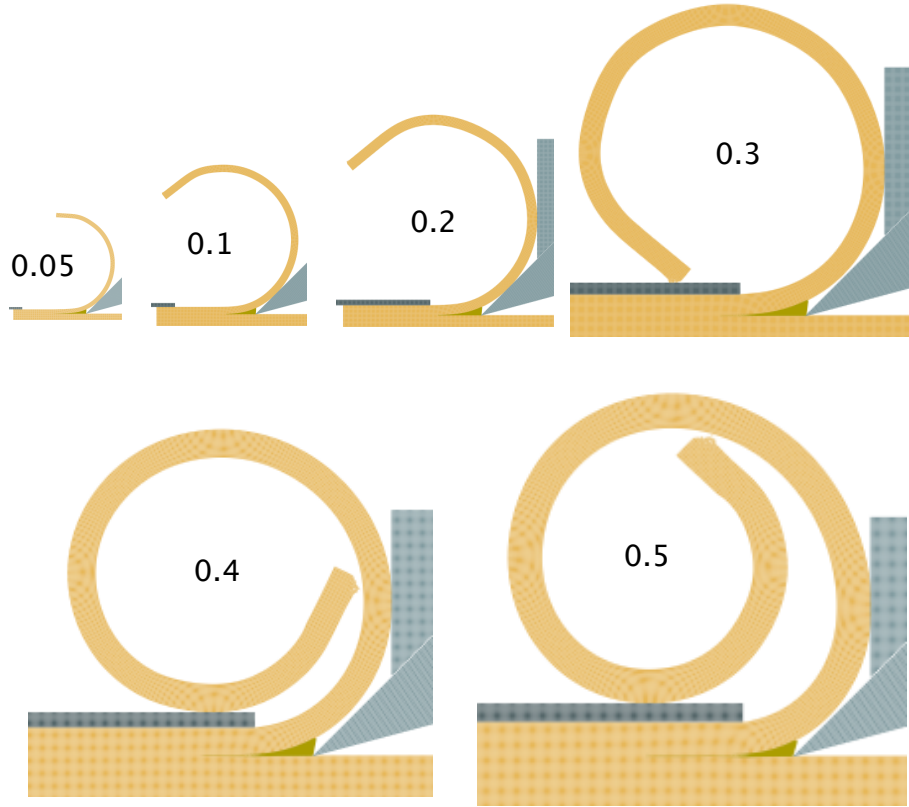


Figure 9. Steady state chips for TL planing with a chip breaker located $b = 1.59$ mm from the tool tip, a fixed $m = 1.2$ mm mouth opening and various depths of cut (as indicated in mm).

before reaching the chip breaker, while the chip breaker contacts, and therefore alters the chip for all other depths of cut. Starting at about 0.3 mm, the chip breaker/mouth opening combinations caused the chip to lose contact with the tool. In these frictionless simulations, this loss of contact eliminates all vertical force on the tool. The tool/chip breaker combination has only horizontal force while the base plate carries only vertical force. Although more simulations are required to optimize all settings, these simulations show that both chip breaker location and mouth opening should be adjusted whenever the depth of cut is changed. As the depth of cut gets thinner, the chip breaker needs to be moved closer to the tool tip otherwise it serves no purpose. Assuming that the tool should contact the chip to provide the best cut quality, for a given chip breaker location, the mouth opening must either be wide enough to retain that contact (see $m/d > 4$ for $d < 0.3$ mm in Fig. 9), or narrow enough to control chip curvature without using a chip breaker (see $m/d = 1.5$ in Fig 8). The latter option also gets the tool tip the closest to the crack tip, which may or may not be advantageous for high quality cuts.

Figure 10 shows the cutting force as a function of depth of cut for the chips in Fig. 9, which used constant $m = 1.2$ mm (unfilled square symbols). Unlike all cutting models for a bare tool (e.g., Figs. 5 and 7) and for experiments with a bare tool, where cutting forces increase linearly or less than linearly, these cutting forces increased (empirically) exponentially as a function of depth of cut. The solid line shows a fit to exponential increase of $F_c/B = Ae^{kd}$ where $A = 233$ J/m² and $k = 6.72$ mm⁻¹. The intercept (A) is close to the mode I initiation toughness (as indicated on the plot). To test if the exponential increase for thick cuts is caused by lower m/d for thick cuts,

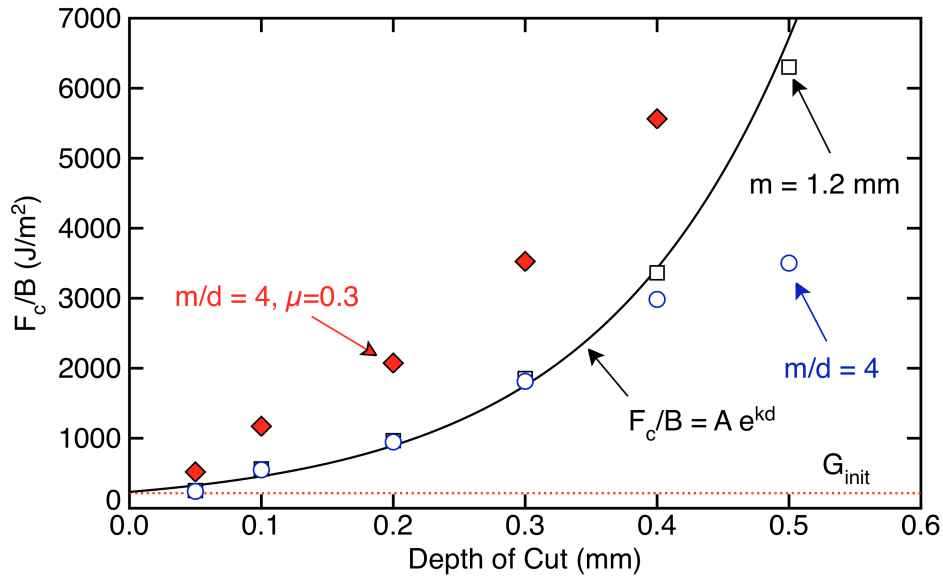


Figure 10. Cutting force, F_c , per unit width (B) as a function of depth of cut for TL planing for conditions shown in Fig. 9 ($m = 1.2$ mm) and for $m/d = 4$ without friction (unfilled symbols) or with friction (filled symbols). The dotted horizontal line shows the mode I initiation toughness. The solid line is exponential fit to cutting forces for $m = 1.2$ mm.

the simulations were repeated for constant $m/d = 4$ (see unfilled circle symbols in Fig. 10). For thin cuts, the cutting force was unchanged because that force is unaffected by $m/d > 4$ (see Fig. 8). For depths of cut 0.4 and 0.5 mm the cutting force is reduced due to larger m/d . The transverse force on the tool was also affected by mouth setting and it increased as m/d decreased. Thus the simulations with $m/d = 4$ had higher transverse force for thin cuts ($d < 0.3$ mm) but lower transverse force for thick cuts ($d > 0.3$ mm).

Grinding Angle

The tool's grinding or bevel angle is set when the tool is ground and sharpened and most bevel-down, bench plane blades are ground to 25° to 30° . Numerical simulations, however, suggest the grinding angle has essentially no effect on cutting performance. Changing that angle from a low value to close the maximum value of 45° in simulations showed no effect on chip formation or on cutting forces. This result was not unexpected. All cutting theories assume that the dominant tool angle variable is the rake angle. The only effect of changing grinding angle at constant rake angle is to change clearance angle, and that angle has much less effect on cutting mechanics. Apart from cutting mechanics, several issues could make the grinding angle important. First, a large grinding angle might eventually lead to more tool rubbing on the cut surface; it is likely that some tool clearance angle is beneficial. Second, a small grinding angle will probably weaken the tool tip resulting in reduced tool durability (this effect cannot be modeled with rigid tools used here). Third, some woodworking planes use a bevel-up tool placement. In this arrangement, the grinding angle would change the rake angle, which would clearly make it an important variable.

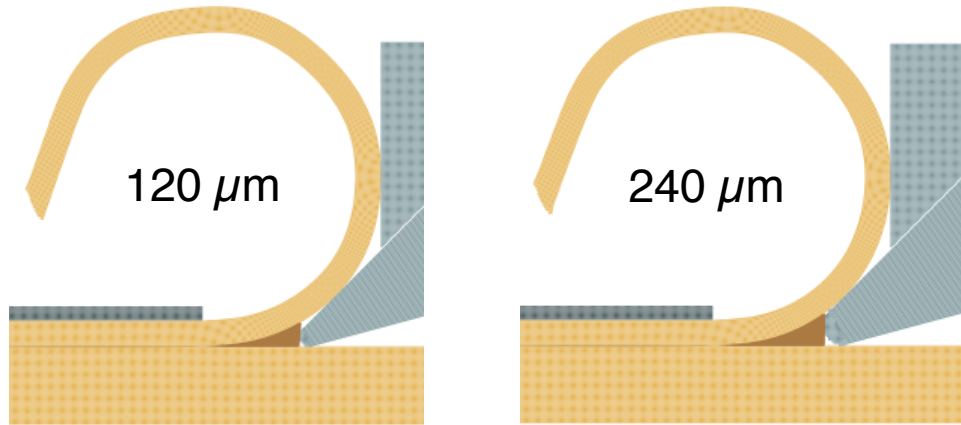


Figure 11. Steady state chips for TL planing with a chip breaker located $b = 1.59$ mm from the tool tip, a fixed $m/d = 4$ mouth opening and depth of cut of 0.3 mm. The two chips are for tools with 120 μm or 240 μm radii.

Tool Sharpness

To simulate tool sharpness effects, the tool's tip was rounded to radii of 60, 120, 180, and 240 μm . Cutting simulations were run for depth of cut $d = 0.3$ mm, chip breaker location $b = 1.59$ mm, and $m/d = 4$. Tool sharpness effects on cutting forces were very small. Comparing a simulation for a sharp tool and one for a blunt, 240 μm radius tool, the cutting forces only increased 5% while the transverse forces on the tool decreased 17%. Figure 11 shows steady state chips for 120 μm and 240 μm radius tool tips to be compared to sharp tool in Fig. 8 (for $m/d = 4$). As seen in these chips, contact between the tool and the chip is about half way between the sharp tool tip and the chip breaker (about 0.8 mm from the tip). Because the region near the tool tip is not contacting the chip, its removal when simulating a blunt tip had very little effect. In all simulations, the tool's leading edge was assumed to cut the bridging fibers when it reached those fibers. The only reason the force increased for blunt tips was that a blunt tool's leading edge reached the cohesive zone later than a sharp tool tip and therefore would cut fewer bridging fibers.

The simulation result that tool sharpness has little or no effect, contrasts with practical woodworking experience that sharp tools cut better. One possibility is that blunt tools, unlike sharp tools, would not be able to cut the bridging fibers. If a blunt tool leaves those fibers intact, or even bends those fibers pulling on the chip surfaces, then blunt tools could result in much higher cutting forces. A second possibility is that all these tools are rather sharp (it was difficult to simulate tools blunter than 240 μm radius tip and still get the tool to start the cutting process). Individual wood cells (or wood fibers) in Douglas-fir wood are hollow cells with diameters around 60 μm [34]. It is unlikely that sharpening tools beyond the dimension of elements in the morphology of the material being cut could improve cutting performance. Perhaps the 240 μm radius tool simulated here corresponds to sufficiently sharp tools in practical woodworking. These two possibilities could be addressed by quantitative comparison to experimental results as a function of tool bluntness.

Effects of Friction

Although all previous simulations used frictionless contact, because a bench plane has much more surface area in contact with the material being cut, it is likely important to account for friction. The filled diamond symbols in Fig. 10 repeat the $m/d = 4$ simulations as a function of depth of cut for friction coefficient equal 0.3 on all contacting surfaces. The forces are nearly double those from simulations with frictionless contact. For depth of cut of 0.5 mm, the forces in the presence of friction were too high to finish a stable simulation. The frictional contact used simple Coulomb friction. It is easy to extend to non-Coulomb friction (such as friction with adhesion [9] or velocity-dependent coefficient of friction). The exploration of such laws is best coupled to experimental results for metal/wood frictional properties.

Finally, note that all simulations *vs.* depth of cut are consistent with extrapolation of F_c/B to zero depth of cut being equal to the material's toughness. Here the extrapolations are close to the initiation toughness because the tool has cut most of the bridging fibers. Furthermore, the tool cuts more bridging fibers for thin cuts because the tool gets closer to the crack tip. An experimental challenge when doing extrapolations is how best to extrapolate cutting forces. The exponential extrapolation worked well for $m = 1.2$ mm, but that was purely an empirical observation. For constant $m/d = 4$ (with or without friction), the simulations results look close to linear, but a linear extrapolation to zero depth of cut gives a large uncertainty. Perhaps rather the trying to develop methods for extrapolating experimental results to zero depth of cut, a better approach would be to couple numerical simulations to experiment results at various depths of cut and find toughness by inverse simulation procedures.

Conclusions

This numerical modeling combined the long-held belief that cutting is determined by elastic-plastic properties of the chip and frictional properties of the contact surfaces with the newer concept that surface energy (or fracture properties of the cut material) also plays a significant role [1,4]. These concepts were implemented in Material Point Method (MPM) simulations to take advantage of that method's capabilities for handling explicit cracks, complex contact conditions, and large displacements and rotations. Accepting the implementation concepts and modeling details, the MPM simulations are best viewed as an experimental method, albeit a virtual one. The virtual experimental results for a bench plane show that chip breaker location, mouth opening, and depth of cut are interrelated suggesting that the former two should be adjusted whenever the depth of cut is changed. More simulations would be needed before modeling could recommend how they should be adjusted. Other results suggest that grinding angle is unimportant and tool sharpness plays a secondary role in cutting forces for tip radii under 240 μm .

The ability to model a complex process such as wood planing, suggests a future potential to address other areas in wood machining such as non-orthogonal cutting, sawing, drilling, and veneer peeling. Two important questions to answer when modeling wood machining are to determine the conditions that provide the highest quality cut surfaces and, for some problems, to determine the conditions that give the lowest energy process. The answer to such questions will likely require coupling of experiments to modeling. Once experimental conditions are found for high-quality or low-energy cuts, numerical simulation results can be interrogated to determine which details of cutting force or other simulation output correlate with those desirable machining qualities.

Acknowledgements

This work was supported by the National Institute of Food and Agriculture, United States Department of Agriculture, under McIntire-Stennis account #229862, project #OREZ-WSE-849-U.

References

1. Atkins, A. (2003). Modelling metal cutting using modern ductile fracture mechanics: Quantitative explanations for some longstanding problems. *International Journal of Mechanical Sciences*, 45(2):373 – 396.
2. Atkins, A. (2004). Rosenhain and Sturney revisited: The “tear” chip in cutting interpreted in terms of modern ductile fracture mechanics. *Proceedings of the Institution of Mechanical Engineers, Part C: Journal of Mechanical Engineering Science*, 218(10):1181–1194.
3. Atkins, A. (2005). Toughness and cutting: A new way of simultaneously determining ductile fracture toughness and strength. *Engineering Fracture Mechanics*, 72(6 SPEC ISS):849–860.
4. Atkins, A. G. (2009). *The Science and Engineering of Cutting*. Butterworth-Heinemann, Oxford.
5. Wyeth, D. J. and Atkins, A. G. (2009). Mixed mode fracture toughness as a separation parameter when cutting polymers. *Eng. Fract. Mech.*, 76(18):2690–2697.
6. Patel, Y., Blackman, B., and Williams, J. G. (2009). Determining fracture toughness from cutting tests on polymers. *Engineering Fracture Mechanics*, 76(18):2711 – 2730.
7. Gamonpilas C, Charalambides M. N., Williams J. G. (2009) Determination of large deformation and fracture behaviour of starch gels from conventional and wire cutting experiments, *J. Material Science*, 44:4976-4986.
8. Semrick, K. (2012). Determining fracture toughness by orthogonal cutting of polyethylene and wood-polyethylene composites. MS Thesis, Oregon State University, Corvallis, OR, USA.
9. Williams, J. G., Patel, Y., and Blackman, B. R. K. (2010). A fracture mechanics analysis of cutting and machining. *Engineering Fracture Mechanics*, 77(2):293–308.
10. Williams, J. G. (2011). The fracture mechanics of surface layer removal. *Int. J. Fract.*, 170:37–48.
11. Nairn, J. A. (2015). Numerical simulation of orthogonal cutting using the material point method. *Engineering Fracture Mechanics*, 149:262–275. (doi:10.1016/j.engfracmech.2015.07.014)
12. Sulsky, D., Chen, Z., and Schreyer, H. L. (1994). A particle method for history-dependent materials. *Comput. Methods Appl. Mech. Engrg.*, 118:179–186.
13. Sulsky, D., Zhou, S.-J., and Schreyer, H. L. (1995). Application of a particle-in-cell method to solid mechanics. *Comput. Phys. Commun.*, 87:236–252.
14. Sadeghirad, A., Brannon, R. M., and Burghardt, J. (2011). A convected particle domain interpolation technique to extend applicability of the material point method for problems involving massive deformations. *Int. J. Num. Meth. Engng.*, 86(12):1435–1456.
15. Nairn, J. A. (2003). Material point method calculations with explicit cracks. *Computer Modeling in Engineering & Sciences*, 4:649–664.
16. Guo, Y. and Nairn, J. A. (2004). Calculation of j-integral and stress intensity factors using the material point method. *Computer Modeling in Engineering & Sciences*, 6:295–308.

17. Guo, Y. and Nairn, J. A. (2006). Three-dimensional dynamic fracture analysis in the material point method. *Computer Modeling in Engineering & Sciences*, 16:141–156.
18. Bardenhagen, S. G., Guilkey, J. E., Roessig, K. M., Brackbill, J. U., Witzel, W. M., and Foster, J. C. (2001). An improved contact algorithm for the material point method and application to stress propagation in granular material. *Computer Modeling in Engineering & Sciences*, 2:509–522.
19. Lemiale, V., Hurmane, A., and Nairn, J. A. (2010). Material point method simulation of equal channel angular pressing involving large plastic strain and contact through sharp corners. *Computer Modeling in Eng. & Sci.*, 70(1):41–66.
20. Nairn, J. A. (2013). Modeling of imperfect interfaces in the material point method using multimaterial methods. *Computer Modeling in Eng. & Sci.*, 92(3):271–299.
21. Bodig, J. and Jayne, B. A. (1982). *Mechanics of Wood and Wood Composites*. Van Nostrand-Reinhold Co, Inc., New York.
22. Forest Products Laboratory (2010). *Wood handbook: wood as an engineering material*. General technical report FPL-GTR-190. Madison, WI: U.S. Dept. of Agriculture, Forest Service, Forest Products Laboratory.
23. Nairn, J. A. (2007). A numerical study of the transverse modulus of wood as a function of grain orientation and properties. *Holzforschung*, 61:406–413.
24. Hill, R. (1948). A theory of the yielding and plastic flow of anisotropic metals. *Proc. Roy. Soc. London, Series A. Mathematical and Physical Sciences*, 193(1033):281–297.
25. Fung, Y. C. (1965). *Foundations of Solid Mechanics*. Prentice-Hall International, Inc.
26. Ayton, G., Smondyrev, A. M., Bardenhagen, S. G., McMurtry, P., and Voth, G. A. (2002). Interfacing molecular dynamics and macro-scale simulations for lipid bilayer vesicles. *Biophys J*, 83:1026–1038.
27. Nairn, J. A. (2009). Analytical and numerical modeling of R curves for cracks with bridging zones. *Int. J. Fract.*, 155:167–181.
28. Bardenhagen, S. G., Nairn, J. A., and Lu, H. (2011). Simulation of dynamic fracture with the Material Point Method using a mixed J-integral and cohesive law approach, *Int. J. Fracture*, 170:49-66. (doi 10.1007/s10704-011-9602-1).
29. Nairn, J. A. (2015). Material Point Method and Finite Element Method Software Package – OSUPDocs. http://osupdocs.forestry.oregonstate.edu/index.php/Main_Page.
30. Williams, J. G. (1989). End corrections for orthotropic DCB specimens. *Comp. Sci. & Tech.*, 35:367–376, 1989.
31. Matsumoto, N., and Nairn, J. A. (2012). Fracture toughness of wood and wood composites during crack propagation. *Wood and Fiber Science*, 44(2):121–133.
32. Shir Mohammadi, M., and Nairn, J. A. (2014). Crack Propagation and fracture toughness of solid balsa used for cores of sandwich composites, *Journal of Sandwich Structures and Materials*, 16 (1): 22-41.
33. Yang, Q. D., and Thouless, M. D. (2001). Mixed-mode fracture analysis of plastically-deforming adhesive joints, *International Journal of Fracture* 110 (2):175–187.
34. Haygreen, J. G., and Bowyer, J. L. (1996). *Forest Products and Wood Science: An Introduction*. Iowa State University Press, Ames, Iowa, USA.